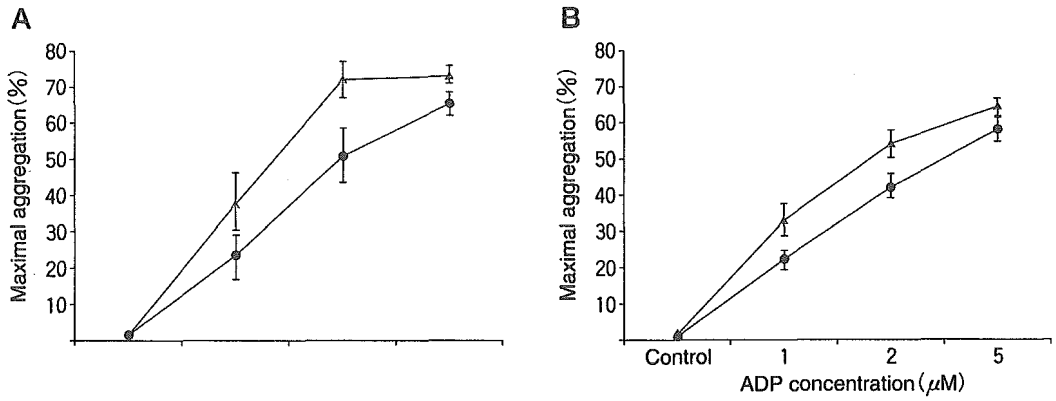

図5　ADP 受容体遺伝子多型と血小板機能の関連

1、2、または 5μmol/L ADP による最大凝集率を示す．
▲：H2 haplotype を有する個体(n = 10)．●：H2 haplotype を有さない個体(n = 10)．A：クエン酸添加 PRP，B：ヒルジン添加 PRP．

(文献 9 より引用)

が提唱されているが，どれも決定的ではない．上述した遺伝子多型が血小板機能の個体差やアスピリンをはじめとする抗血小板薬の感受性に影響する可能性が十分に考えられ，今後の研究に期待が寄せられる．

References

1) 松本興治，広瀬　一，林　勝知，他：術後深部静脈血栓症に関する研究．静脈学 **5**：163-170，1994
2) O'Donnell CJ, Larson MG, Tofler GH, et al：Genetic and environmental contributions to platelet aggregation：the Framingham heart study. Circulation **103**：3051-3056, 2001
3) Kunicki TJ, Kritzik M, Nugent DJ, et al：Hereditary variation in platelet integrin α2β1 density is associated with two silent polymorphisms in the α2 gene coding sequence. Blood **89**：1939-1943, 1997
4) 村田　満，松原由美子：遺伝子多型と疾患―血栓症―．血液，免疫，腫瘍 **6**：63-70，2001
5) 村田　満：動脈血栓症と血小板膜糖蛋白遺伝子多型．日本内科学会雑誌 **89**：47-54，2000
6) Murata M, Matsubara Y, Ikeda Y, et al：Coronary artery disease and polymorphisms in a receptor mediating shear stress-dependent platelet activation. Circulation **96**：3281-3286, 1997
7) Matsubara Y, Murata M, Ikeda Y, et al：Platelet glycoprotein Ib alpha polymorphisms affect the interaction with von Willebrand factor under flow conditions. Brit J Haematol **128**：533-539, 2005
8) Feng D, Lindpaintner K, Larson D, et al：Increased platelet aggregability associated with platelet GPIIIa PlA2 polymorphism. The Framingham offspring study. Arterioscler Thromb Vasc Biol **19**：1142-1147, 1999
9) Fontana P, Dupont A, Gaussem P, et al：Adenosine diphosphate-induced platelet aggregation is associated with P2Y12 gene sequence variations in healthy subjects. Circulation **108**：989-995, 2003

血栓性血小板減少性紫斑病

鈴木美佐子　村田 満

概念

血栓性血小板減少性紫斑病（thrombotic thrombocytopenic purpura ； TTP）は1924年にMoschcowitzが初めて報告した疾患で血小板減少，細小血管障害性溶血性貧血，腎機能障害，発熱，動揺性精神神経症状の五徴候を特徴とする（表1）．一方，TTPとの鑑別が問題となる溶血性尿毒症症候群（hemolytic uremic syndrome ； HUS）は血小板減少，細小血管障害性溶血性貧血，腎機能障害を主徴とする疾患である．

TTPとHUSは臨床症状と病態の類似性から血栓性細小血管障害（thrombotic microangiopathy ； TMA）として1つのカテゴリーに属する疾患とされていた．その後，TTPの病因はvon Willebrand因子切断酵素（VWF-cleaving protease ； VWF-CP, a disintegrin-like domain, and metalloproteinase, with thrombospondin type 1 motif 13 ； ADAMTS13）の活性低下であることが判明した．図1にTTPの発症機序を示す．先天性TTPではVWF-CP（ADAMTS13）の遺伝子変異により酵素活性が欠損しており，後天性TTPではVWF-CP（ADAMTS13）に対してIgG型の自己抗体が存在するためにその酵素活性が低下，このため患者血漿中に超高分子量VWF複合体が存在，血小板血栓を心臓，腎臓，脳などの細小動脈に形成する．

表1　TTPの五徴

- 血小板減少
- 細小血管障害性溶血性貧血
- 腎機能障害
- 発熱
- 動揺性精神神経症状

病型分類，病因論的事項

表2に示すようにTTPは発症様式から家族性である先天性と非家族性である後天性に大別される．先天性TTPは遺伝的にVWF-CP（ADAMTS13）活性が低下しており，インヒビターの存在によってVWF-CP（ADAMTS13）活性が低下している後天性TTPとは区別される．先天性TTPのうち出生直後から重症の新生児黄疸を認め，血小板減少や溶血性貧血を反復する早期発症型はUpshaw-Schulman症候群（USS）と呼ばれる．また，成人になるまで無症状で，妊娠や感染を契機に発症する成人発症型の先天性TTPもある．後天性は原因不明である特発性と膠原病，悪性疾患，

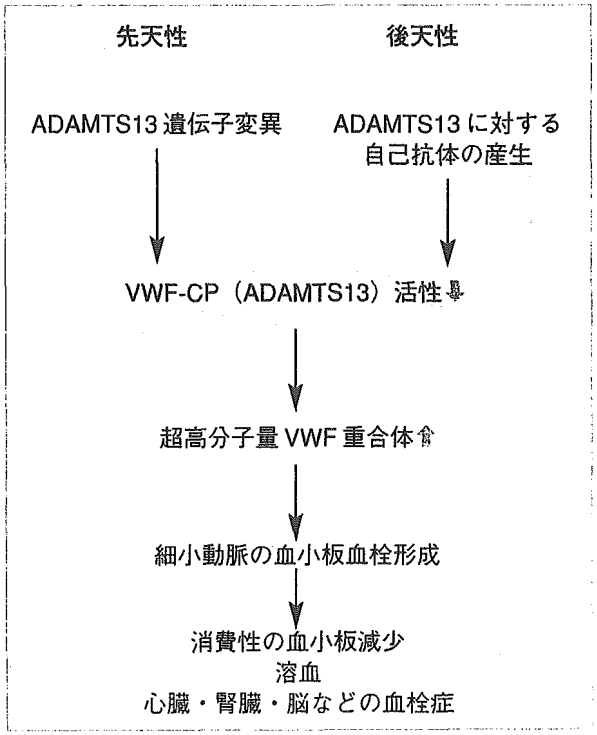

図1　TTPの発症機序

造血幹細胞移植，薬物（チクロピジン，バイアグラ®），ウイルス感染症や妊娠などに合併する二次性TTPに分類されている．

主要症状

TTPに特徴的な症状としては前述の五徴として①点状出血，紫斑，歯肉出血，皮下出血などの血小板減少による出血傾向，②貧血症状，黄疸，血色素尿などの溶血性貧血症状，③腎機能障害（10％程度は急性腎不全に移行），④38℃前後の発熱，ときに40℃を超える高熱，⑤幻覚，妄想，せん妄，錯乱，意識障害，頭痛，四肢麻痺，構語障害，失語症，知覚障害，痙攣などの不安定で動揺する精神神経症状が挙げられる．消費性血小板減少による出血傾向はほぼ全例にみられる．精神神経症状はTTPの90％において認められ，HUSとの鑑別に重要である．

主要検査成績

細小血管障害性溶血性貧血

細小血管障害性溶血性貧血は免疫学的機序によらない溶血性貧血でありクームス試験は陰性である．末梢血液像における破砕赤血球や断片化赤血球（red cell fragmentation）の出現，赤芽球，網状赤血球の増加，血清乳酸脱水素酵素，間接ビリルビン値の増加，血清ハプトグロビン値の減少などの所見がみられる．特に“fragmentation”は本疾患に特徴的所見であり，診断に非常に重要である．ただし破砕赤血球や断片化赤血球は症状出現後24～48時間は末梢血に出現しないことがあり留意する必要がある．

表2　TTPの病型分類

先天性	後天性
ADAMTS13遺伝子異常（Upshaw-Schulman症候群）	ADAMTS13活性の低下を伴うもの ・特発性 ・薬剤 ・妊娠 ・HIV感染 ・自己免疫疾患 ・血管内リンパ腫（IVL） ・肝疾患 ADAMTS13活性の低下があまりみられないもの ・造血幹細胞移植 ・悪性腫瘍

血小板数の低下

TTPの患者において消費性血小板数低下は必ずみられる所見である．

腎障害

TTPにおける腎障害では，中等度のタンパク尿を認めることが多い．尿中に細胞成分や円柱，尿潜血や赤血球円柱が認められることは少ない．

VWF-CP（ADAMTS13）活性とインヒビター

血漿を用いてVWF-CP（ADAMTS13）活性とインヒビターを測定する方法としてはVWFマルチマー解析に加え蛍光基質を用いたFRETS-VWF73が開発されている．後者に関しては間もなく大手検査センターで検査受託が開始されるものと思われる．

わが国での報告においても，後天性TTPのうち特発性TTPではVWF-CP（ADAMTS13）活性は著減しており，高率にインヒビターを認めている．二次性TTPではインヒビターが存在し酵素活性が低下していたのは，薬物性と妊娠合併TTPであり，造血幹細胞移植や悪性腫瘍に合併するTTPでは酵素活性低下は軽度で自己抗体が存在しないものが多い．膠原病性TTPでは酵素活性は著減から正常まで様々で，インヒビターの陽性率も約50％であった．VWF-CP（ADAMTS13）活性，インヒビター測定はTTP／HUSの診断上非常に有用な検査ではあるが，これによる明確な病型分類は難しい．従来のように臨床症状の差異，すなわち精神神経症状の有無を重視してTTPとHUSの鑑別を行うべきと考えられている．

診断

先天性TTPの診断

前述の五徴に加え，VWF-CP（ADAMTS13）に対するインヒビターを認めずVWF-CP（ADAMTS13）活性の著減をみた場合，先天性TTPを疑い，既往歴ならびに家族のVWF-CP（ADAMTS13）活性測定を行う．近年続々とADAMTS13遺伝子変異が報告されており，今後，ADAMTS13遺伝子解析が診断に貢献するようになると思われる．

後天性TTPの診断

前述のようにVWF-CP活性ならびにその自己抗体価の測定法の確立はTTPの診断に大きく貢献しているものの，現時点では迅速検査が一般化されていない．実際の臨床の現場では早急な診断，治療開始が必須であり臨床症状からTTPを疑い，早期に血漿交換を導入し，症状経過をみていく．すなわち臨床症状，経過とVWF-CP（ADAMTS13）活性，自己抗体価の測定結果を総合し，TTPとHUS，播種性血管内凝固症候群（disseminated intra-vascular coagulopathy ； DIC）の鑑別ならびにTTPの病型分類を行う必要がある．

鑑別診断

TTP，HUSならびにDICでは広範な微小血管内血栓形成により，臓器の循環障害をきたし，類似した臨床症状を示す．

HUSは血小板減少による下痢，血便などの出血傾向，溶血性貧血および急性腎不全を特徴とするが，TTPとの鑑別が困難な症例もしばしばみられる．

DICの症状はTTP，HUSと同様の出血症状に加え臓器症状として，脳神経症状（昏睡，痙攣），循環器症状（ショック），呼吸器症状（ARDS），腎症状（無尿，乏尿），消化器症状（消化性潰瘍，壊死に伴う下血），貧血があるが基礎疾患による症状との判別が難しい．DICにおいて認められる検査所見としては，①血液凝固亢進（トロンビン・アンチトロンビン複合体の高値，可溶性フィブリンモノマー陽性，D-ダイマー高値），②二次線溶亢進（プラスミン・α_2プラスミン・インヒビター複合体の高値，血清FDP値の上昇），③血栓形成に伴う血小板，凝固線溶因子などの消費亢進（血小板数減少，血漿フィブリノーゲンの減少，プロトロンビン時間の延長），④臓器の循環不全を反映するものが挙げられる．

TTPとHUSにおいては血小板減少を認める点ではDICと共通であるが，血液凝固亢進や二次線溶亢進の所見や凝固線溶因子などの消費亢進が認められることは少なく，この点がDICとTTP，HUSを鑑別する上で重要である．

治療

先天性TTPの治療法

治療法としては新鮮凍結血漿（FFP）の輸注によりVWF-CPの補充を行うことが唯一の治療法である．USSでは2～3週に1度FFPの輸注を反復継続している症例が多い．一方，成人発症型のTTPでは発作時のみのFFP輸注を要する場合が多い．

後天性TTPの治療法

◉血漿交換

TTPは血漿交換が治療法として確立される以前は極めて予後不良の疾患と考えられてきたが，現在では発症早期から血漿交換を行うことで予後の改善傾向を認めている．血漿交換は患者血漿中の自己抗体と同時に血小板と反応する超高分子量VWF多量体をも除去し，不足しているVWF-CP（ADAMTS13）を補充する効果，ならびに血管内皮障害や血小板活性化を助長する高サイトカイン血症を改善する効果がある．VWF-CP（ADAMTS13）活性の著減のない症例でも血漿交換の有効性は認められており，発症早期から血漿交換を開始し病勢が安定するまで連日行うことが重要である．新鮮凍結血漿（FFP）で通常40～60ml / kg / 回の血漿交換を施行する．治療効果は血小板数の回復，精神神経症状の回復，

LDH値の改善により判定可能であるが，血漿交換を中止するとすぐに再燃する症例もあり，血漿交換の間隔を徐々にあけ血漿交換からの離脱を図っていき，中止時期については慎重な判断を要する．血漿輸注は自己抗体価が低ければ中和に有効であるが，高力価であれば効果は乏しく，適応の見極めを要する．

◉副腎皮質ステロイド

副腎皮質ステロイドはTTPが自己免疫疾患であることが明らかとなる以前から，経験的に血漿交換と併用されてきた．自己抗体であるVWF-CP（ADAMTS13）インヒビターの抑制効果がある．

◉免疫抑制薬

血漿交換に抵抗性を示す難治例や慢性再発性TTPでは免疫抑制薬併用の有効性が報告されているが，初期治療としての血漿交換との併用については，有効性について今後の検討を要する．副腎皮質ステロイド同様，VWF-CP（ADAMTS13）インヒビターの抑制効果が期待される．ビンクリスチン，シクロスポリン，アザチオプリン，シクロホスファミドなどの報告がある．

最近では，悪性リンパ腫の治療に使われるCD20に対するキメラ抗体であるリツキシマブが慢性再発性TTPに対し有効であると報告されている．ただしいずれの薬剤も現時点では保険適用外であり，難治例に対する治療法として今後さらなる検討が必要である．

◉抗血小板薬

TTPは諸臓器の細小動脈における血小板血栓形成に基づいており，TTP患者血漿には血小板凝集亢進作用があることが報告されている．このため抗血小板薬の有効性が考えられ，血漿交換，副腎皮質ステロイドとの併用で用いられている．ただし出血を助長する可能性があり，出血傾向の強い症例では避けた方がよい．

◉脾臓摘出

血漿交換に抵抗性を示す難治例や慢性再発性TTPでは脾臓摘出が奏功したという報告があるが適応症例の選択は慎重にすべきである．VWF-CP（ADAMTS13）インヒビターを産生するBリンパ球の重要な産生場所が除かれることによる効果と考えられる．

予後

TTPは血漿交換が治療法として確立される以前，致死率は90％にのぼり極めて予後不良の疾患と考えられてきたが，血漿交換により18％程度に減少している．しかし血漿交換抵抗性の症例や，慢性再発性，難治性の症例があり，今後，ベッドサイドでの簡便な診断法や治療法の確立による予後の改善が期待される．

文献
1）松本雅則，八木秀男，藤村吉博：vWF-cleaving protease／ADAMTS13．臨床血液 2003；44：159-167.
2）鈴木美佐子，池田康夫：血液浄化療法．日本臨床増刊号 2004；62：482-485.

日本医師会生涯教育シリーズ

わかりやすい免疫疾患

本書は日本医師会生涯教育シリーズ-67（日本医師会雑誌 第134巻・特別号(1)／
平成17年6月15日刊）として刊行された同名の雑誌をそのまま単行本化したものです．

2005年6月15日　第1版第1刷

監修・編集　宮坂信之
編　集　小池隆夫・住田孝之・山本一彦
羅　智靖・渡辺　守・石井裕正

発　行　日本医師会
〒113-8621　東京都文京区本駒込2-28-16
電話（03）3946-2121（代表）

会　長／植松治雄
副 会 長（生涯教育担当）／櫻井秀也
常任理事（生涯教育担当）／橋本信也
事務局長／熊谷冨士雄

編集・制作　日本医師会生涯教育課　編集企画室
制作協力　株式会社 南山堂／後藤亮弘・窪田雅彦・秋山孝子
発　売　株式会社 南山堂　代表者　鈴木　肇
〒113-0034　東京都文京区湯島4丁目1-11
電話　編集(03) 5689-7850・営業(03) 5689-7855
振替口座　00110-5-6338
印刷・製本　図書印刷株式会社

●日本医師会の生涯教育シリーズは，生涯教育用テキストとして各方面から高い評価を得ております．
●継続して御購読頂くためには是非日本医師会への加入をお勧めします．

乱丁・落丁の場合はお取り替えいたします．
ISBN 4-525-16761-0　Printed in Japan

A16761101-A

UltraRapid Communication

Carbon Monoxide From Heme Oxygenase-2 Is a Tonic Regulator Against NO-Dependent Vasodilatation in the Adult Rat Cerebral Microcirculation

Mami Ishikawa,* Mayumi Kajimura,* Takeshi Adachi, Kayo Maruyama, Nobuya Makino, Nobuhito Goda, Tokio Yamaguchi, Eiichi Sekizuka, Makoto Suematsu

Abstract—Although the brain generates NO and carbon monoxide (CO), it is unknown how these gases and their enzyme systems interact with each other to regulate cerebrovascular function. We examined whether CO produced by heme oxygenase (HO) modulates generation and action of constitutive NO in the rat pial microcirculation. Immunohistochemical analyses indicated that HO-2 occurred in neurons and arachnoid trabecular cells, where NO synthase 1 (NOS1) was detectable, and also in vascular endothelium–expressing NOS3, suggesting colocalization of CO- and NO-generating sites. Intravital microscopy using a closed cranial window preparation revealed that blockade of the HO activity by zinc protoporphyrin IX significantly dilates arterioles. This vasodilatation depended on local NOS activities and was abolished by CO supplementation, suggesting that the gas derived from HO-2 tonically regulates NO-mediated vasodilatory response. Bioimaging of NO by laser-confocal microfluorography of diaminofluorescein indicated detectable amounts of NO at the microvascular wall, the subdural mesothelial cells, and arachnoid trabecular cells, which express NOS in and around the pial microvasculature. On CO inhibition by the HO inhibitor, regional NO formation was augmented in these cells. Such a pattern of accelerated NO formation depended on NOS activities and was again attenuated by the local CO supplementation. Studies using cultured porcine aortic endothelial cells suggested that the inhibitory action of CO on NOS could result from the photo-reversible gas binding to the prosthetic heme. Collectively, CO derived from HO-2 appears to serve as a tonic vasoregulator antagonizing NO-mediated vasodilatation in the rat cerebral microcirculation. (*Circ Res.* **2005;97:e104-e114.**)

Key Words: carbon monoxide ■ heme oxygenase ■ diaminofluorescein ■ nitric oxide ■ NO synthase ■ vascular tone

Carbon monoxide (CO) has attracted much interest since implicated as a gaseous messenger for neural and vascular systems.[1–3] This diatomic gas displays considerable similarities as well as differences with NO, an established gaseous mediator.[4] In view of gas-generating mechanisms, CO is synthesized by heme oxygenase (HO), the enzyme executing oxidative cleavage of protoheme IX into biliverdin IXα. This reaction is similar to that of NO synthase (NOS) in that both require NADPH as an electron donor and molecular oxygen as cosubstrates. HO resembles NOS because both involve constitutive and inducible isozymes; the latter is induced by a similar spectrum of stressors such as hypoxia and cytokines.[5,6] Another common property is a vital role played by the heme in catalytic reactions of these enzymes. Whereas in the NOS, the heme is incorporated within the protein interior, HO is unique because the substrate (ie, protoheme IX) also serves as a catalytic center constituting oxygen activation. In this respect, its enzyme–substrate complex but not HO alone forms a transient heme protein. Considering such properties of gas-generating reactions, one gas can interfere with generation of another through multiple mechanisms. First, the two reactions could compete for using NADPH and molecular oxygen. Second, enhanced HO reaction could reduce the amount of heme in cells,[7] causing a reduction in the enzymatic activity of NOS. Finally, in vitro, CO and NO can bind to the heme of NOS and of the HO–substrate complex, respectively; therefore, it could inhibit the reactions.[8–10]

Such a property that the two gases bind to the ferrous heme with high affinity could be targeted not only to gas-generating enzymes but also to other receptor proteins possessing the heme. Consequently, it provides both gases a point to interact with each other to effect functions of receptor proteins in vivo.[11,12] One example of this cross-interaction of the two gases on one receptor is soluble guanylate cyclase (sGC), to which heme either NO or CO can bind to increase its activity,

Original received October 1, 2005; revision received October 27, 2005; accepted November 9, 2005.

From the Department of Biochemistry and Integrative Medical Biology (M.I., M.K., T.A., K.M., N.M., N.G., M.S.) and Department of Neurosurgery (M.I.), School of Medicine, Keio University, Tokyo, Japan; Department of Molecular Genetics and Biochemistry (T.Y.), Tokyo Medical and Dental University, Japan; and Department of Internal Medicine (M.I., E.S.), Saitama National Hospital, Japan.

*Both authors contributed equally to this study.

Correspondence to Makoto Suematsu, MD, PhD, Professor and Chair, Department of Biochemistry and Integrative Medical Biology, School of Medicine, Keio University, Tokyo 160-8582, Japan. E-mail msuem@sc.itc.keio.ac.jp

Circulation Research is available at http://circres.ahajournals.org DOI: 10.1161/01.RES.0000196681.34485.ec

although the potency of CO is far less than that of NO in vitro.[12–14] Such interactions among the gas-producing or receptor systems could give rise to complex cellular and tissue responses that determine the final functional outcome in vivo.

In this context, molecular mechanisms whereby CO and NO modulate the vascular tone in vivo have not completely been understood. In the liver, where endogenous NO production appears low,[2,11] CO is abundantly produced, and its cancellation by inhibiting the HO activity or capturing the gas directly causes sinusoidal constriction, indicating that the gas is necessary to maintain low vascular resistance in this organ.[2,3,15,16] In other organs producing relatively high NO, inhibitory effects of CO on the NO-mediated sGC activation have also been plausible; the transgenic mice with site-specific HO-1 overexpression in vascular smooth muscle cells (VSMCs) displayed systemic hypertension,[17] suggesting that HO-1–derived CO interferes with activation of sGC by endothelium-derived NO. Likewise, in the cerebral circulation, the effect of CO on vascular tone remains controversial.[18,19] The reason why the effect of CO in the very same organ varies among different studies has been unclear; however, the key to solve this inconsistency could lie in examining spatial relationship or anatomical proximity between gas-producing sites and their reception sites in the tissue that has been left from careful examination.

This study thus aimed to determine effects of suppressing endogenous CO derived from HO on local NO production and to relate those with changes in arteriolar tone. In addition to conventional immunohistochemical approaches, spatiotemporal information of local NO generation in the presence or absence of the CO suppression was collected in vivo directly with laser-confocal intravital microscopy. The results suggest that distinct from its action in the liver, CO is a tonic regulator against NO-dependent vasodilatation in the cerebral microcirculation of the adult rat.

Materials and Methods

General and Cranial Window Preparations

The procedures described in this article have been performed with the approval of the Animal Care and Use Committee of Keio University School of Medicine. Experiments were performed on male Wistar rats (280 to 350 g; CLEA Japan; Tokyo, Japan) that were not fasting before experiments. Rats were anesthetized with an intraperitoneal injection of α-chloralose (60 mg/kg) and urethane (600 mg/kg), tracheostomized, and spontaneously ventilated. The femoral artery and vein were cannulated for monitoring mean arterial pressure (MAP) and sampling arterial blood for the blood gas analysis. Rectal and window temperature were monitored and kept at 36°C to 37°C with the use of a thermostatically controlled heating lamp. The head of each rat was fixed in a stereotaxic frame, and the left parietal bone was exposed by a longitudinal midline skin incision. After three polyethylene tubes (PE-50; ID, 0.58 mm; OD, 0.965 mm) were fixed on the skull with cyanoacrylate, a closed cranial window was made with the use of a cover glass and quick self-curing acrylic resin (GC Unifast). The pial surface was then superfused with artificial cerebrospinal fluid (CSF); its composition was (mmol/L): 147.8 Na^+, 3.0 K^+, 2.3 Ca^{2+}, 135.2 Cl^-, 19.6 HCO_3^-, 1.67 lactate, 1.1 phosphate, and 3.9 glucose, equilibrated with 5% CO_2 and 5% O_2 balanced with N_2 at 37°C. The MAP, arterial CO_2 partial pressure (P_{CO2}), and arterial blood pH were kept within the normal range during experiments (Table).

Arterial Blood Pressure, Gases, and pH

	n	MAP (mm Hg)	pH	P_{CO2} (mm Hg)	P_{O2} (mm Hg)
Pre-experiment	25	109±2	7.41±0.03	32±4	86±14
Post-experiment	25	105±2	7.41±0.05	31±3	89±15

Values are mean±SD.

Immunohistochemical Analysis

Anesthetized rats were transcardially perfused with PBS for 5 minutes to remove blood. The specimens were fixed in paraformaldehyde-lysine-periodate solution at 4°C for 4 hours, cryoprotected, and embedded in optimal cutting temperature compound (Miles Laboratories). Coronal sections with 8-μm thickness were prepared at −20°C and incubated with optimal concentrations of antibodies. GTS-1 and GTS-2 are monoclonal antibodies (mAbs) raised against rat HO-1 and HO-2, respectively in our laboratory.[15] We also applied mAb 24G, which recognizes bilirubin (BR)–IXα[20]; because BR-IXα is generated from biliverdin-IXα, a regiospecific product of HO reactions, 24G7-specific immunoreactivities serve as a marker of HO-mediated degradation of heme and CO generation in vivo. Semiserial sections were also stained with mAbs against NOS1 and NOS3 (Transduction Laboratories), sGC (Wako Chemicals), and syntaxin (Sigma). These primary antibodies were detected by streptavidin/horseradish peroxidase–coupled secondary antibody (Vectastain Elite ABC kit; Vector Laboratories, Inc) and diaminobenzidine as a chromogen.

Determinations of Isozyme-Specific HO Activities and BR-IXα Content

HO activities were determined by measuring formation of BR-IXα as described previously.[21] To determine the HO-1–specific activity, we used GTS-3, an anti-rat HO-1 mAb, prepared in our laboratory. Microsomal fractions were prepared, and 50 μL of the microsomal samples were incubated with the same volume of either PBS or GTS-3 (0.5 mg/mL). When GTS-3 was added to the reaction mixture, it blocks the HO-1–specific enzyme activity with relatively low dose.[22] Total HO activity was determined by measuring BR-IXα production in the presence and absence of GTS-3.

BR-IXα content in CSF and effluents collected from superfusate were determined by an ELISA using mAb 24G7.[23]

Direct Detection of NO Production in the Pial Microcirculation

The pial microcirculation was observed through a cranial window with an upright microscope (Olympus BX51W1) using either a 20× (XLUMPlanFl, NA; 0.95) or a 40× (LUMPlanFl, NA; 0.8) water immersion lens. The microscopy was equipped with a silicon-intensified target camera (C2400–08; Hamamatsu Photonics) and a real-time laser-confocal imaging system (CSU21 confocal scanner; Yokogawa, Inc.) assisted by an 8-bit digital processor. Values for gain and offset of the camera as well as those for the laser-power supply were constant throughout the experiments.

To visualize NO-producing sites in vivo, diaminofluorescein-2 diacetate (DAF-2DA; Daiichi Pure Chemicals Co Ltd), an NO-sensitive fluoroprobe,[24,25] was superfused on the pial surface. The 60-minute superfusion of DAF-2DA (10 μmol/L) caused no significant elevation of adherent venular leukocytes. To collect microfluorographs of the NO-associated fluorescence, the pial surface was epi-illuminated by an excitation wavelength of 488 nm with a short exposure time <0.5 s at 20 and 60 minutes. The microscopic fields containing an unbranched segment of the arteriole (15 to 40 μm in diameter) were selected, and only those that shared the same focusing plane were examined.

To examine the spatial distribution of DAF-2 probe, we also used 4-aminofluorescein (4-AF) diacetate (Calbiochem), an NO-insensitive fluorophore. Because 4-AF cannot react with NO by forming a triazole-ring, its fluorescence intensity is insensitive to the

presence of NO; therefore, it has been used as a negative control for DAF-2. Fluorescence intensities of the two separate anatomical locations were quantified; at the arteriolar wall and at the extravascular cells located in the subarachnoid space. For the arteriolar wall, ≈400 measurements were taken as a single line-scan along the longitudinal axis of the vessel wall and 5 longitudinal line-scans with 0.4-μm steps between lines were taken and averaged. Therefore, a scanned area formed of ≈400×5 pixels represented 150×2 μm^2 in real space. For the extravascular cells, a size variable window (120×10 μm^2 in real space on average) was positioned at the area that shared the same focusing plane with the vessel walls.

Calibration of the fluorescence intensities was performed by determining gray levels of known concentrations of DAF-2 triazole (DAF-2T; Daiichi Pure Chemicals Co Ltd), a stable compound yielded by the interaction between DAF-2 and NO^+. The collected images were processed by the digital imaging software (MetaMorph 6.1; Universal Imaging Corporation), and the pixel-based data in the area of interest were converted into gray levels. Based on the calibration line, gray levels were converted into the corresponding concentrations of DAF-2T, designated as apparent DAF-2T concentrations ($DAF\text{-}2T_{app}$) at 20 minutes and 60 minutes. As an index of local NO production, the rate of elevation of $DAF\text{-}2T_{app}$ during this 40-minute (DAF-NO formation) was calculated using the following formula: DAF-NO formation $(nmol \cdot L^{-1} \cdot min^{-1}) = ([DAF\text{-}2T]_{app\ at\ 60\ minutes} - [DAF\text{-}2T]_{app\ at\ 20\ minutes})/40$ minutes.

NO Measurements in Cultured Porcine Aortic Endothelial Cells

Porcine aortic endothelial cells (PAECs) were harvested and cultured on type I collagen-coated dish in M199 medium supplemented with 10% FBS as reported.[26] NO production in cultured PAECs between passages 6 and 10 was assessed using the DAF-2DA as described previously.[25] Briefly, PAECs at 95% confluence were serum-depleted for 2 hours in DMEM containing HEPES (22 mmol/L). Cells were incubated with DAF-2DA (10 μmol/L) at 37°C for 20 minutes as the basal dye loading, and followed by 30-minute dye loading for measurements of DAF-NO formation. The NO formation was determined by calculating fractional changes in fluorescence intensities measured at 50 minutes versus those measured at 20 minutes. The fractional changes in the NO formation were expressed as values versus the controls, which were treated with the vehicle-containing medium. To examine actions of CO on the endothelial NO generation, tricarbonyldichlororuthenium (II) dimer (100 μmol/L; Sigma), a CO-releasing molecule (CORM), was added at 30 minutes before the basal dye loading. To test whether the effect of CO resulted from its specific binding to heme proteins, cells in the dishes were exposed to white light, which was provided by a fiber light guide equipped with a metal halide lamp (PMH-160; 150 W; Mejiro Precision) that covers wavelengths between 400 and 800 nm.[27,28] The experimental rig and the imaging systems were the same as those used for the study in vivo. At least 20 to 30 individual cells per dish were analyzed, and more than three separate sets of experiments were conducted for each group. Distinct from other gases with the heme-binding ability such as O_2 and NO, CO can be dissociated from the prosthetic heme easily on light exposure.[27,28] This experiment thus allowed us to prove whether the effect of CO on the NO generation resulted from the specific gas binding to the heme proteins, including NOS.

Using the same PAECs after depleting serum for 24 hours, immunoblotting of NOS3 and its phosphorylated form were performed according to previous methods.[26] Briefly, 30 to 40 μg of total protein was diluted in Laemmli buffer containing 5% β-mercaptoethanol, denaturated 5 minutes at 95°C, separated by SDS-PAGE (10% gels), and transferred onto polyvinylidene difluoride membranes. Membranes were saturated in PBS with 0.05% Tween 20 and 3% nonfat milk for 1 hour. Blocked membrane was incubated with an antibody directed against phospho-NOS3 (Ser-1177, Cell Signaling Technology) or that against NOS3 (Transduction Laboratories) at a dilution of 1:1000 in the same buffer for overnight at 4°C. Membrane was rinsed with PBS with Tween 20 and incubated with the horseradish peroxidase–conjugated secondary antibody for 1 hour. Proteins were detected with an ECL reagent on an x-ray film. When necessary, cells were treated with CORM or $RuCl_3$ at desired concentrations for 1 hour. H_2O_2, a reagent known to elicit phosphorylation of NOS3, was added at 200 μmol/L for 1 hour as a positive control.[26]

Statistics

Values are expressed as means±SE unless mentioned. Significant differences between means were evaluated using ANOVA followed by Fisher's test for multiple comparisons. Differences indicating P values <0.05 were considered statistically significant.

Results

Cell-Specific Localization of Gaseous Monoxide-Generating Systems in the Rat Cerebrum

To determine the distribution of CO- and NO-generating systems in the cerebrum, immunohistochemical analysis was performed. Appreciable HO-2 immunoreactivities were found in subdural mesothelial cells, arachnoid trabecular cells, the arteriolar endothelium in the subarachnoid space, and neural cells in parenchyma (Figure 1A and 1F). Immunoreactivities for NOS3 (Figure 1D and 1H) were clearly demonstrated in the endothelium, whereas those of NOS1 (Figure 1C and 1G) appeared to be almost indistinguishable from those of HO-2, indicating that the sites of CO production coincide with those of NO production. Likewise, such colocalization of HO-2 and NOS1 was evident in the hippocampal neuron (Figure 1J through 1N). To confirm whether expressed HO-2 degrades protoheme-IX to produce CO and, if so, to identify sites of CO production, the tissue was stained for BR-IXα, an end product of HO-mediated heme degradation. Figure 2 illustrates cell-specific distribution of gas-producing and reception sites in the vicinity of an arteriole. Immunoreactivities of mAb 24G7 indicated that BR-IXα occurred in arteriolar endothelia, VSMCs, and arachnoid trabecular cells, indicating actual CO generation by HO in these cells. BR-IXα was also detected in the CSF (0.8±0.2 μmol/L; n=6) and became immeasurable by the replacement with artificial CSF for 60 minutes. These results suggest that local heme degradation and CO generation by HO occurred in and around pial microvascular systems. Collectively, the site of HO activity indicated by BR-IXα appeared to overlap not only with that of NOS3 but also in part with that of NOS1. It should be noted that the tissue did not exhibit any notable immunoreactivities of HO-1 (data not shown).

To determine the isozyme-specific HO activities, mAb GTS-3 was used to inhibit HO-1–dependent activities. When mAb GTS-3 was added to the reaction mixture of the brain samples, it did not cause any reduction in the total HO activity compared with the basal activity measured in the presence of IgG (Figure 2F). On the other hand, adding mAb GTS-3 to the spleen sample substantially reduced the HO activity by ≈75% (Figure 2G), consistent with our previous observation in the rat spleen showing the activity ratio between HO-1 and HO-2 is ≈3:1.[22] Therefore, it appears that HO-2 is a major source for the catalytic activity of the enzyme in the brain, and HO-1 plays little role, if any, at least under normal conditions. Together, these results suggest that

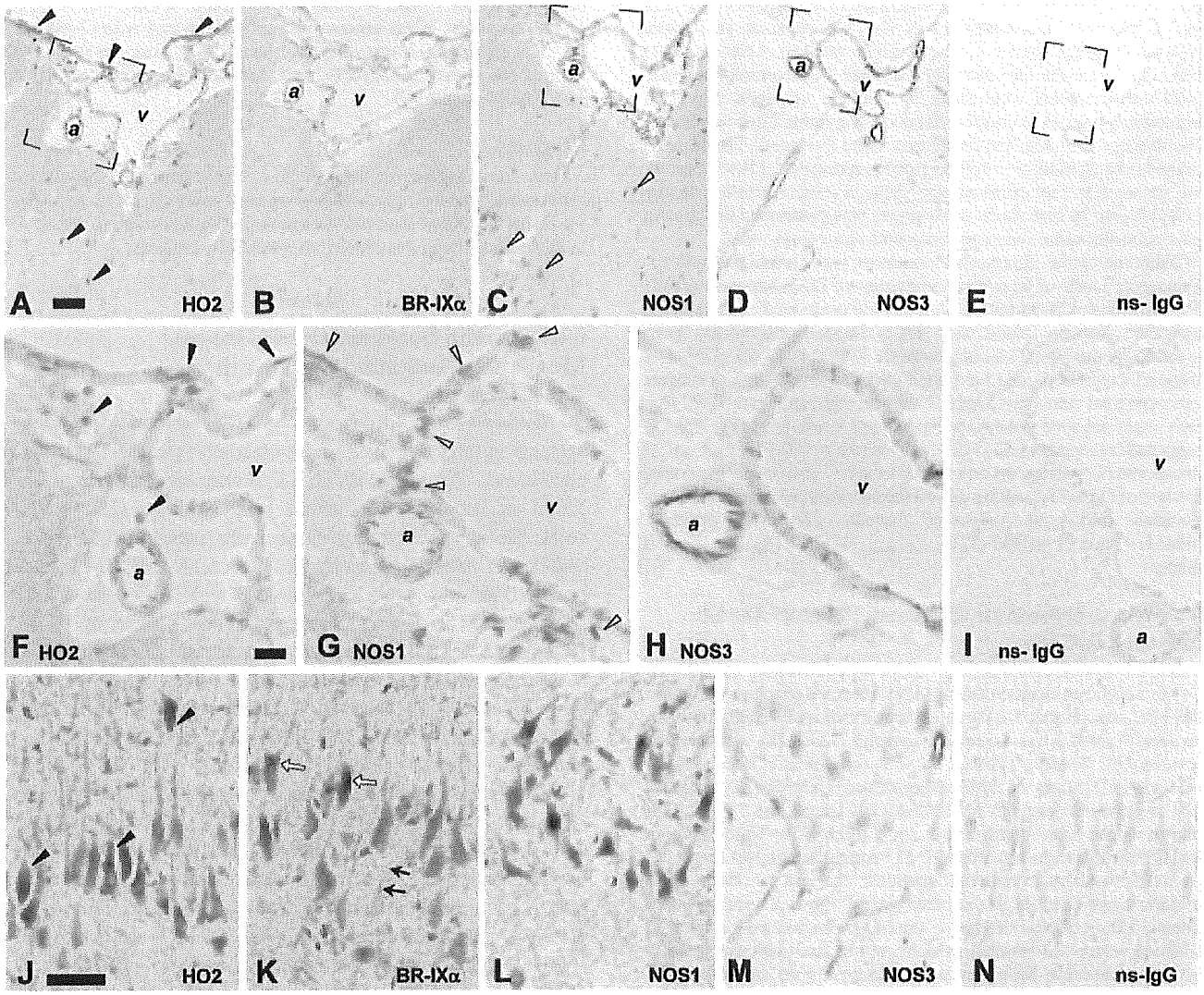

Figure 1. Distribution of CO- and NO-producing enzymes in the rat brain. A, Immunohistochemical staining for HO-2 in a coronal section of the cerebrum. Note strong labeling at subdural mesothelia and somata in the cortex (black arrowheads). B, Immunoreactivity for BR-IXα is weak but similar to those with HO-2. C, NOS1 immunoreactivity is similar to that of HO-2. Somata in the cortex show pronounced labeling of NOS1 (white arrowheads). D, NOS3 immunoreactivity is confined to the endothelium. Square marked by brackets in A, C, D, and E indicates the field shown in F, G, H, and I, with high magnification. F and G, Thin cells forming the subdural mesothelium and polygonal cells with round nuclei of the trabeculae exhibit strong labeling of HO-2 (black arrowheads) and of NOS1 (white arrowheads). H, Clear labeling of NOS3 is seen in the endothelium. J, Somata in the pyramidal layer of the hippocampus are HO-2 positive (black arrowheads). K, Some somata (white arrows) and processes of neurons (black arrows) are immunopositive for BR-IXα. L, Neurons demonstrate strong labeling for NOS1. M, Clear vascular labeling for NOS3. E, I, and N, Negative controls stained with nonspecific mouse IgG. Bars=50 μm in A and 30 μm in F and J. a indicates arteriole; v, venule.

pial arterioles reside in the environment where sources of CO and NO production are abundant. Interestingly, VSMCs of these vessels are juxtaposed luminally with endothelia and abluminally with arachnoid cells in which enzymatic sources of CO and NO colocalize.

Endogenous CO Suppression Elicits Vasodilatation of Cerebral Arterioles

To examine whether CO plays a role in regulating vascular tone, we attempted to inhibit endogenous CO production by zinc protoporphyrin IX (ZnPP), a competitive inhibitor of HO, and monitored changes in diameter of pial arterioles over a 60-minute period. Superfusion of ZnPP (0.01 to 1 μmol/L) caused a dose-dependent dilatation of pial arterioles. The ZnPP-induced dilatation occurred acutely, being noticeable at as early as 10 minutes after the start of its superfusion at 0.1 μmol/L. The highest dose (1.0 μmol/L) of the inhibitor induced a robust dilatation (54±5% at 60 minutes), whereas the same dose of copper protoporphyrin (CuPP), which does not block the HO activity, caused no significant changes (Figure 3A and 3B). Such dilatation elicited by the CO suppression was significantly reduced by supplementing CO (10 μmol/L) locally. Furthermore, this dilatation by the HO inhibition appears NO-dependent because N^{ω}-nitro-L-arginine methyl ester (L-NAME; 1 mmol/L) but not N^{ω}-D-nitro-arginine methyl ester (D-NAME; 1 mmol/L), attenuated the response (Figure 3C). To note is that a CO-free vehicle superfusion caused a small but notable dilatation (5.9±3.6%

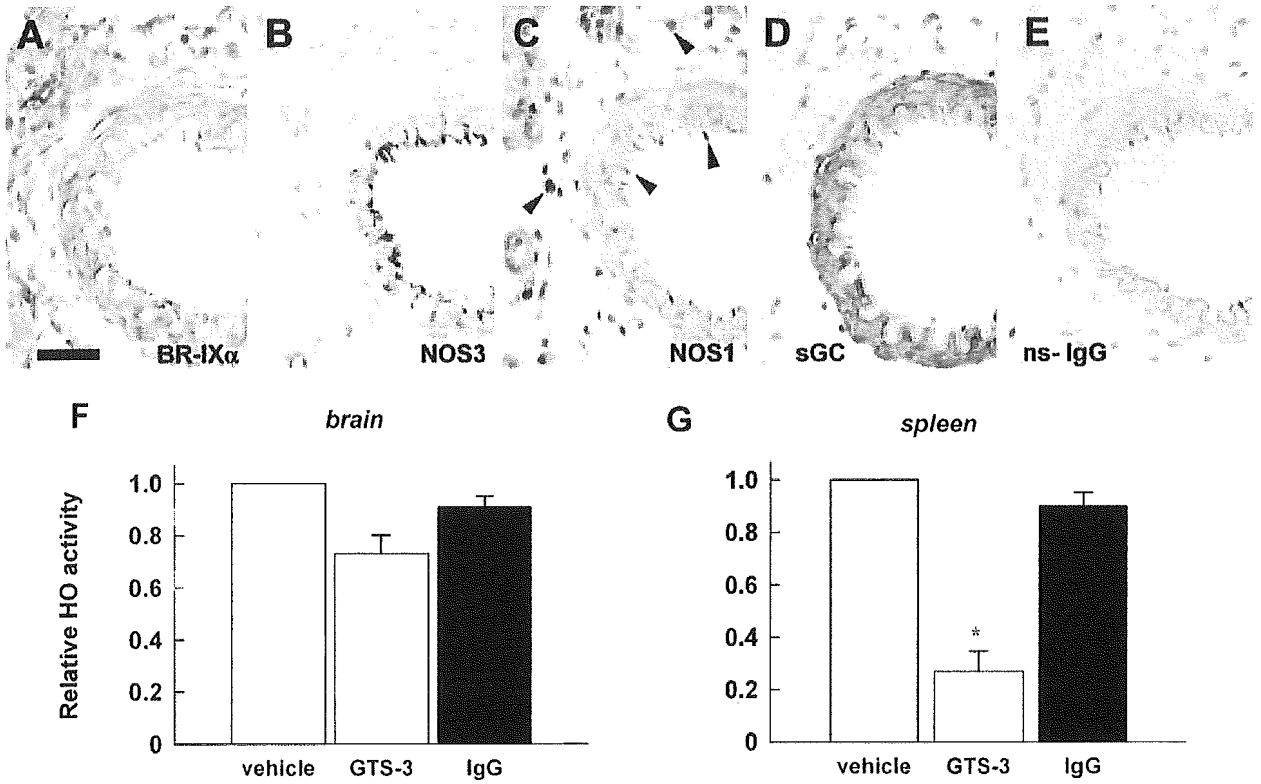

Figure 2. Cell-specific distribution of gas-producing and reception systems in the vicinity of an arteriole. A, BR-IXα immunoreactivities occur in different cells including endothelia, VSMCs, and arachnoid trabecular cells. Bar=30 μm. B, Endothelia exhibit concentrated labeling for NOS3. C, Part of endothelia and arachnoid trabecular cells demonstrate labeling for NOS1 (black arrows). D, sGC is expressed in VSMCs. E, A negative control stained with nonspecific mouse IgG. F and G, Isozyme-specific inhibition of HO activities using GTS-3, a mAb against rat HO-1. Note that GTS-3 suppresses the HO activities of the spleen samples but not of the brain samples. HO activities are expressed as relative values vs the vehicle-treated control. Data represent mean±SE of three separate measurements. *$P<0.05$ compared with the IgG control.

at 60 minutes), and the dilatation was abolished (−0.1±1.9% at 60 minutes) by the superfusion of exogenous CO (10 μmol/L). Such a dilatory event could be a result of eliminating CO in the CSF so far as judged from the local BR-IXα measurements and is consistent with a putative role of this gas acting as a tonic regulator on arteriolar tone.

Three-Dimensional Reconstitution and Quantitative Characterization of NO Generation In Vivo

Aforementioned results suggesting a role of CO in modulating the NO-mediated vasodilatation led us to examine changes in local NO generation quantitatively in and around pial arterioles. Having obtained heterogeneous distribution of gaseous monoxide-generating enzymes even within this thin layer of the arachnoid (Figure 1A through 1I), the assessment must be performed vertically as well as horizontally through the layer. To achieve this prerequisite, we used confocal diaminofluorescein microfluorography to determine spatial and temporal alterations of NO generation in real-time and constructed 3D mapping of the gas. Panel 1 of Figure 4A shows NO-associated fluorescence right below the surface of dura. When the focal plane was moved 20 μm more deeply (panel 2), the arteriolar wall and cells residing in the arachnoid space became more fluorescent. This observation appears to be consistent with the vertical distribution of NOS-positive cells, including endothelia, subdural mesothelial cells, and arachnoid trabecular cells (Figure 1G and 1H). Spatial relationship between panels 1 and 5 of Figure 4A could correspond to the focal planes indicated by the top and the bottom hairlines in Figure 4B. Microvessels residing in the superficial layer lying no more than 100 μm from the dura were subjected to this study. Our methodology allowed us to examine NO generation occurring in these sites. For a series of experiments described in later sections, attention was paid to obtain fluorography focused at the center of the vessel, namely at the point where the largest diameter was seen. By so doing, we could avoid capturing saturated fluorescence that was typically derived from subdural mesothelial cells.

We conducted another control experiment to test whether a constant superfusion of DAF-2DA, an NO capturing reagent, affects vasodilatory response. To do this, we measured arteriolar diameter over a 60-minute period after blocking HO by ZnPP in the presence and absence of DAF-2DA. As seen in Figure 4C, the presence of DAF-2DA (10 μmol/L) significantly blunted vasodilatory response elicited by ZnPP, eliciting a >50% reduction, suggesting that presence of the fluoroprobe restricts the local amount of NO.

The central assumption in the measurement of NO is that a change in a fluorescence intensity represents a proportional change in the number of DAF-2T molecules present in recorded images. We tested this assumption by collecting

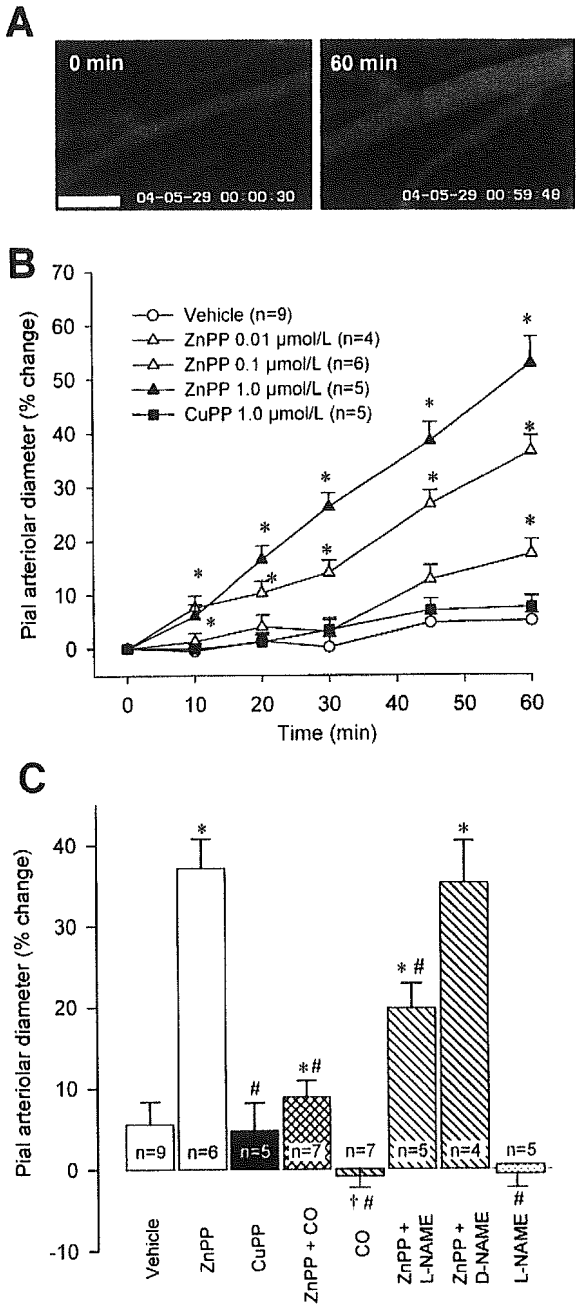

Figure 3. Changes in vasodilatory response on alterations in CO and NO generation. A, Typical changes in arteriolar diameter in response to ZnPP. Bar=100 μm. B, Time course of changes in arteriolar diameter in response to the superfusion of the HO inhibitor at different concentrations. C, Summary data of changes in arteriolar diameter at 60 minutes after the superfusion of various reagents. Supplementation of CO (10 μmol/L) significantly reduces the vasodilatory response induced by the HO inhibition. L-NAME (1 mmol/L) but not D-NAME (1 mmol/L) abolishes this vasodilatation. Diameters are standardized as a percentage of baseline diameters before applying the reagents. *$P<0.05$ an increase compared with the vehicle-treated control. †$P<0.05$ a decrease compared with the vehicle-treated control. #$P<0.05$ compared with the ZnPP-treated group. Values are mean±SE.

fluorescence images from a well filled with DAF-2T in CSF at pH 7.4. Intensities of NO-associated fluorescence were calibrated with known concentrations of DAF-2T. As seen in Figure 4D, the 8-bit gray levels measured through a digital processor were fitted to the second-order polynomial regression. The relationship obtained from three separate measurements was summarized by the following expression: gray level=34.0+0.068 [DAF-2T]+0.0012[DAF-2T]^2 (r^2=0.995).

Suppression of Endogenous CO Stimulates NO Generation and Vasodilatation

To explore the mechanism whereby CO tonically inhibits NO-mediated vasodilatation, we examined the effect of the HO inhibitor on endogenous NO generation using laser-scanning microfluorography. Figure 5A illustrates a series of representative images tracing time-dependent elevation of NO in the pial microcirculation. The first image in the series was taken at 20 minutes after the start of DAF-2DA superfusion; the time just as the vessel wall began to appear fluorescent. In subsequent images taken at 60 minutes, the intensity of fluorescence increased at vascular walls and the cells in extravascular space, suggesting continuous NO generation in these cells. When ZnPP, but not CuPP, was superfused, the DAF-2T fluorescence was already more intense at 20 minutes, and the extent of time-dependent elevation in the fluorescence appeared to be greater than that under the control condition, indicating accelerated production of NO under the CO-suppressed condition. Because not only NO amount but also the esterase activity might determine intensities of the fluorescence, we examined spatial distribution of intracellular esterase activities by loading 4-aminofluorescein diacetate (4AF-DA), an NO-insensitive probe of which the structure is similar to that of DAF-2DA. Unlike spatially heterogeneous elevation of DAF-2T fluorescence, with 4AF-DA, most of arachnoid trabecular cells and microvascular endothelium were stained homogeneously, displaying a pattern of the fluorescence distinct from that with DAF-2DA (Figure 5A, bottom). This observation led us to conclude that a temporal rise in DAF-2T fluorescence was attributed to NO generation, not to the esterase activity.

Figure 5B and 5C summarize quantitative analyses of changes in local NO production expressed as the rate of elevation of DAF-2T$_{app}$ per unit of time. At vascular walls, CO suppression by ZnPP in the tissue, but not by CuPP, caused a significant increase in NO generation approximately by 70%, suggesting that its stimulatory effect on the NO generation results from a specific inhibitory action on HO. Superfusion of CO together with ZnPP completely reversed this elevation to the basal level. To test further whether this effect of CO supplementation was attributable to an inhibitory action on NOS, we simultaneously administered the HO inhibitor with L-NAME. Such a concomitant inhibition of CO- and NO-producing enzymes attenuated the enhanced NO production. When the cells in the extravascular space were examined, altered patterns of changes in NO production were similar to those measured at the vascular walls. However, one distinct point was that CO superfusion caused a more pronounced reduction in NO generation at the extravascular cells than at the vascular walls (45% versus 20%). It may conform to the existence of NO source, which is independent of NOS in circulation.[29] Collectively, these results suggest that CO derived from HO interferes with the NO production.

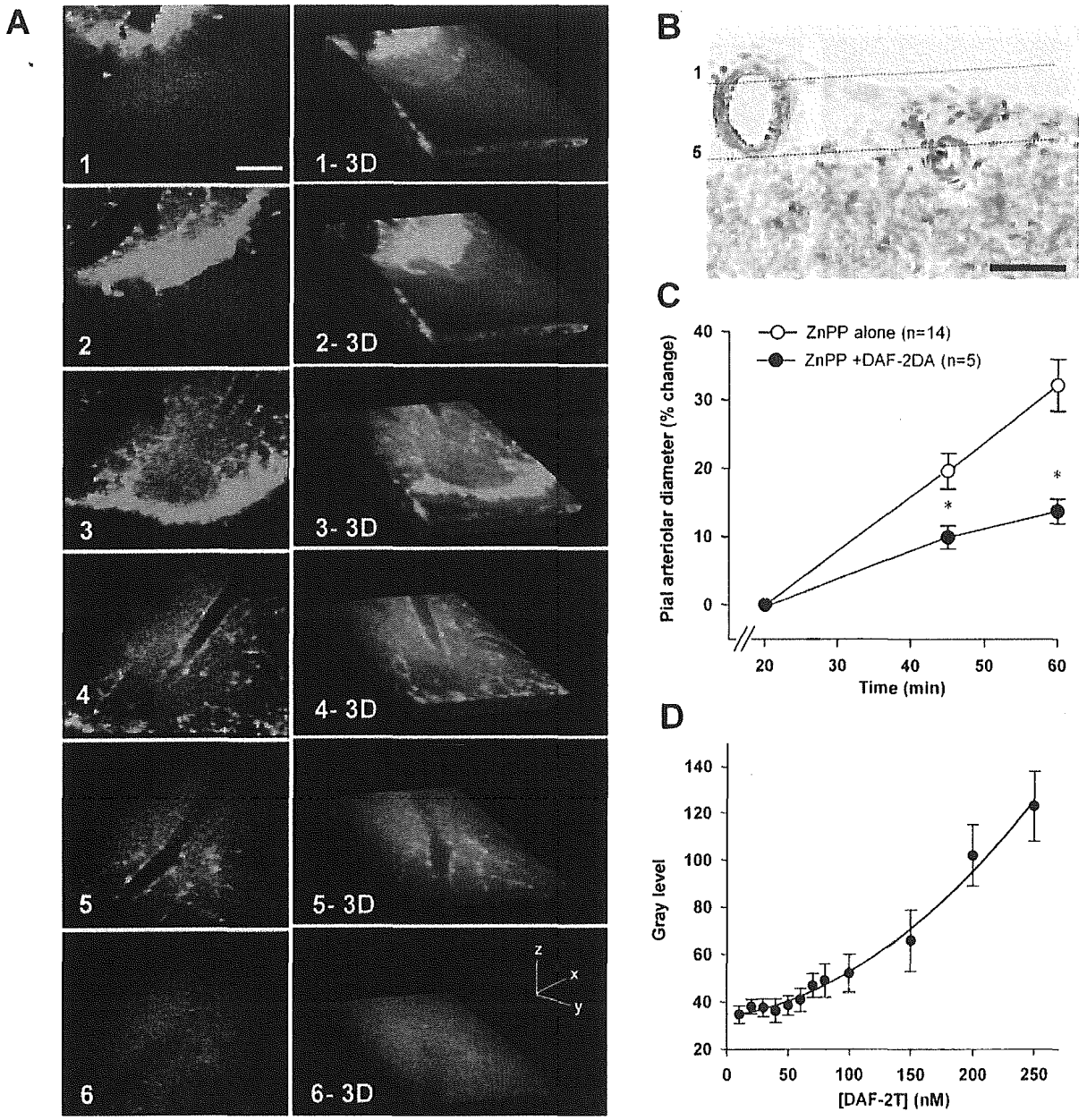

Figure 4. Three-dimensional reconstitution and quantitative characterization of NO generation at the surface of rat cerebrum. A, Two-dimensional images of NO-associated fluorescence at 60 minutes after the start of the DAF-2DA superfusion. At each *x-y* confocal plane, a 2D image is obtained and these images are stacked in sequential order with an imaging software to yield 3D images of the rat cerebral surface. Representative images of six different *x-y* planes covered 150-μm depth of the tissue, and images are either 20 or 30 μm apart. Note that the surface of arachnoid membrane, the cells in subarachnoid space, and the wall of blood vessels exhibit NO-associated fluorescence. Bar=100 μm. B, The section transversing *x-z* plane is incubated with an mAb against syntaxin, an integral protein abundantly expressed in neurons. Arachnoid membrane composed of subdural mesothelial cells and trabecular cells, and the blood vessels are devoid of syntaxin-positive staining, and these cells appear to represent the origin of the fluorescence seen in A. Two parallel lines indicated here could correspond to the spatial relationship between panels 1 and 5 of A. Bar=100 μm. C, The effect of a constant superfusion of DAF-2DA on vasodilatory response induced by the HO inhibition. *$P<0.05$ compared with the group superfused with ZnPP alone. D, The relationship between concentrations of DAF-2T and gray level of the fluorescence intensities is determined in vitro (n=3).

CO Suppresses NO Generation in Cultured Endothelial Cells

To examine mechanisms for CO to antagonize endothelial NO generation, we set out experiments in vitro using PAECs. Likewise to observations in vivo, PAECs displayed a notable NO generation as judged by an increase in DAF-2T fluorescence (Figure 6A, top row). Preincubation with CORM (100 μmol/L) significantly suppressed the NO generation (Figure 6A, middle row; and 6B). The CO-induced changes were cancelled by exposing these cells to white light, whereas the light exposure per se did not alter the basal NO generation. Suppression of the NO generation by CO was unlikely to occur through downregulation of NOS3 expression or that of the enzyme phosphorylation, as judged by immunoblotting

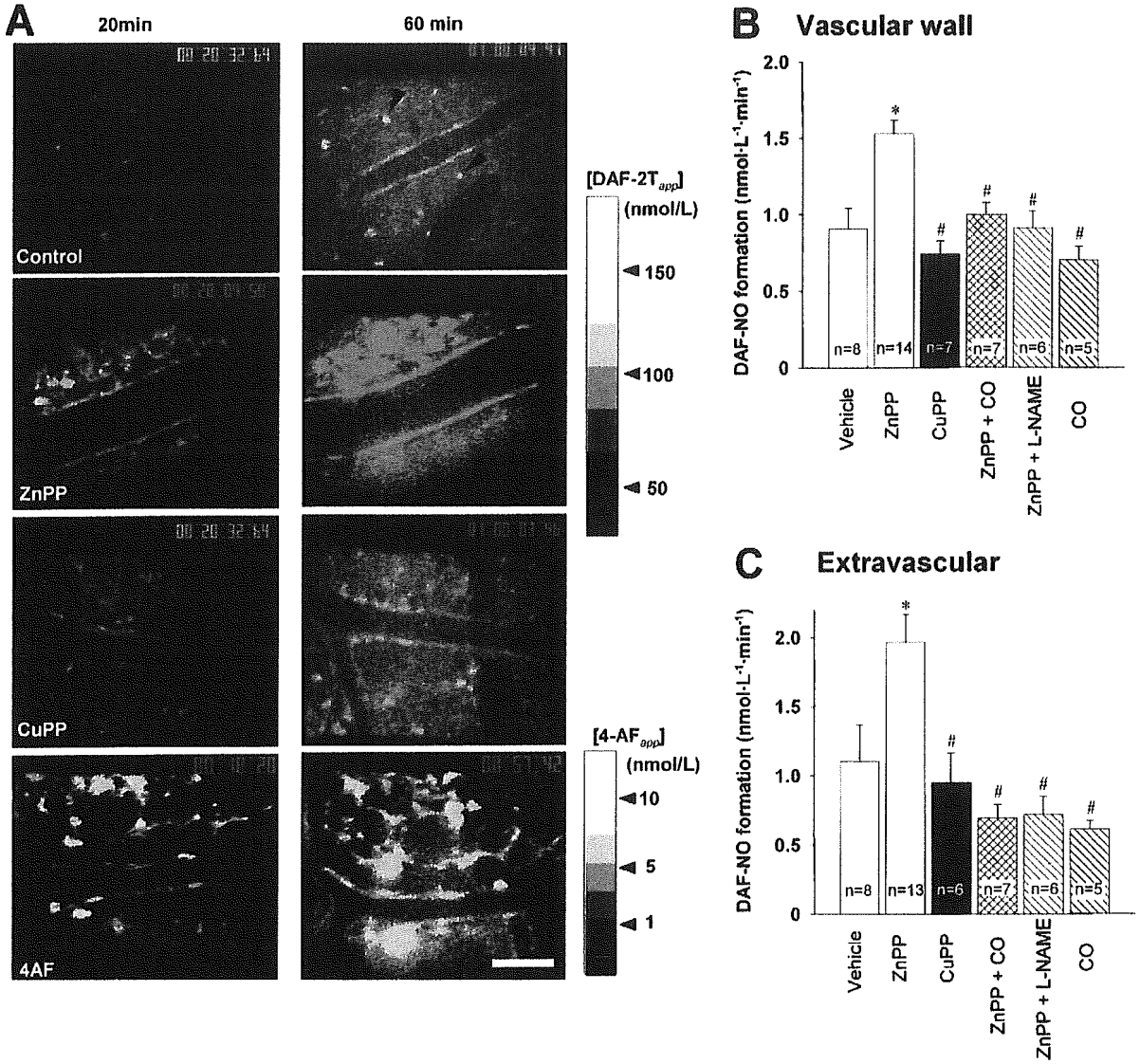

Figure 5. Augmented NO generation under CO-suppressed conditions. A, Time-dependent elevation of NO production in the pial microcirculation. In the control- and the CuPP-treated groups, NO-associated fluorescence is faint at 20 minutes; it then becomes obvious at the vascular walls and at the cells located in extravascular space (arrowheads) at 60 minutes. On the other hand, in ZnPP-treated group, evident fluorescence is exhibited even at 20 minutes, and it increases further at 60 minutes. 4AF-DA, an NO-insensitive fluorescence precursor, is used as a control. B, Quantitative analyses of NO generation at the arteriolar walls. Local gray level intensities measured in vivo are converted to apparent concentrations of DAF-2T (DAF-2T$_{app}$) on the basis of calibration shown in Figure 4D. As an index of local NO formation, rate of elevation of DAF-2T$_{app}$ during this 40-minute (DAF-NO formation) is calculated (see Methods). C, The analyses for the cells located in the extravascular space. *P<0.05 and #P<0.05 compared with the vehicle-treated control and the ZnPP-treated groups, respectively. Values are mean±SE.

using the specific antibodies (Figure 6C). These results suggest that the ability of CO to bind to the prosthetic heme plays an important role in inhibiting endothelial NO generation.

Discussion

Our findings provide evidence that CO produced by constitutive HO can attenuate vasodilatory responses of arterioles by interfering with NO generation in the rat brain. In this study, the physiologic relevance of CO production in cerebral microcirculation is supported by the results of two independent experimental approaches: measurements of pial arteriolar diameter under conditions in which endogenous CO or NO production was varied, and direct detection of NO in situ using the fluoroprobe under normal and CO-suppressed conditions. The use of confocal microscopy together with the immunohistochemical detection of gas-producing enzymes allowed us to obtain spatial and temporal information of CO-modulated NO production in cerebral microcirculation.

There are several mechanisms whereby the HO-CO system modulates NO-dependent biological events. First, inhibition of the HO activity could allow NOS to use intracellular NADPH and O_2 less competitively, thereby causing increased NOS activities. Because NADPH is an intracellular substance that cannot be transported across the cell, HO and NOS are required to reside in the same cell for such a competition to

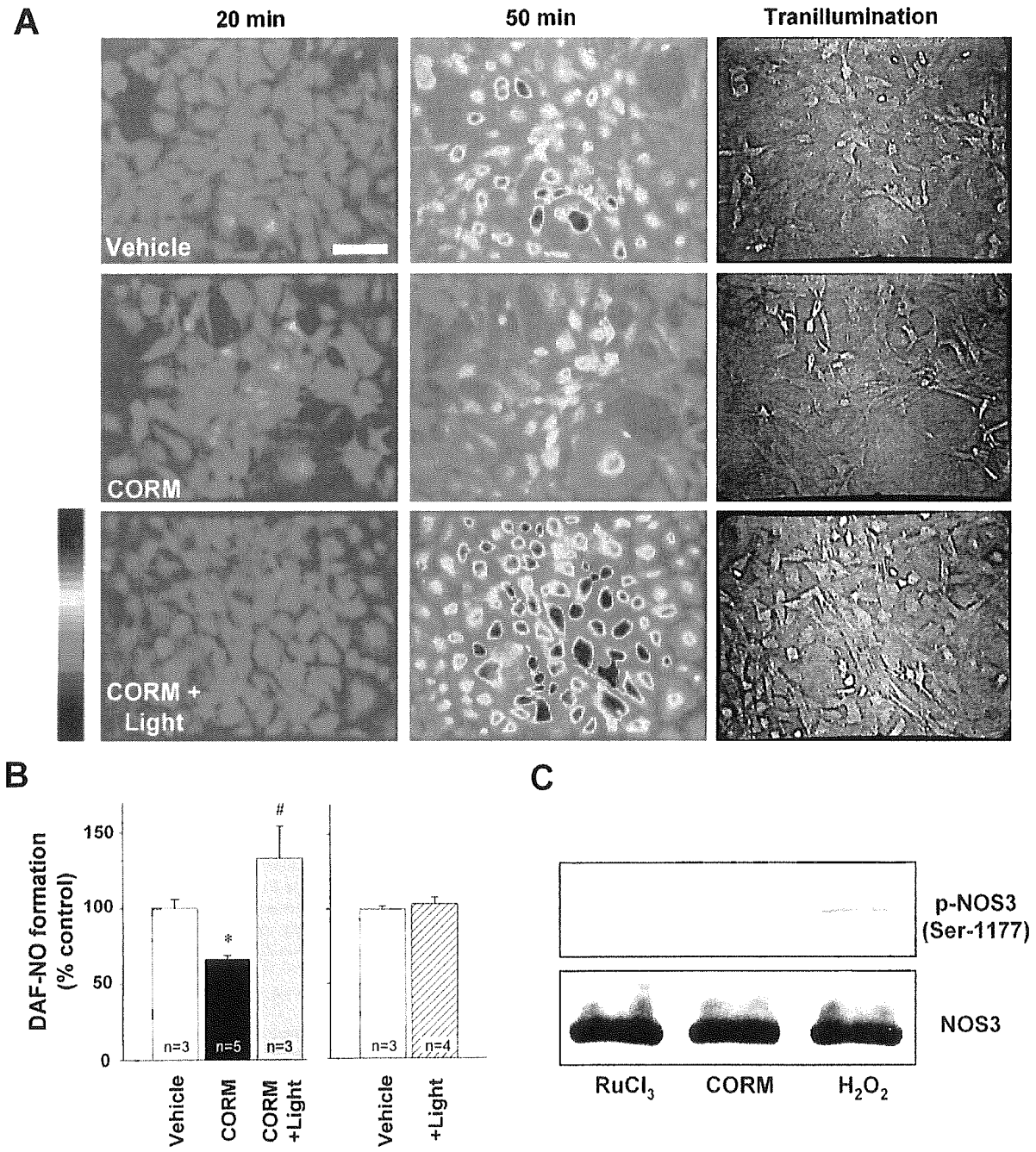

Figure 6. Effects of CORM on NO generation and NOS3 phosphorylation in PAECs. A, Representative fluorescent images of PAECs loaded with DAF-2DA. Left and middle columns, pseudocolor representation of micrographs captured at 20 minutes and 50 minutes after loading of DAF-2DA (10 μmol/L), respectively. Right column, transillumination micrographs after each experiment. Treatment with CORM (middle row) attenuates the basal DAF-NO formation (top row), and this attenuation is cancelled by exposure to white light in the presence of CORM (bottom row). Bar=100 μm. A color bar showing blue, green, yellow, and red indicates the increasing fluorescence intensities. B, Fractional changes in fluorescence intensities indicative of NO production. Data were collected from ≈20 to 30 individual cells from each experiment. Values are mean±SE from 3 to 5 separate experiments. *$P<0.05$ and #$P<0.05$ compared with the vehicle-treated control and the CORM-treated groups, respectively. C, Effects of CORM on expression of NOS3 and phospho-NOS3. PAECs were treated with $RuCl_3$ (100 μmol/L), CORM (100 μmol/L), or H_2O_2 (200 μmol/L), a reagent eliciting the enzyme phosphorylation, for 1 hour. Cell proteins were obtained and eNOS expression and phosphorylation of eNOS at Ser1179 were determined with the immunoblotting. Representative for 4 independent experiments.

take place. Second, oxidative degradation of heme by HO could downregulate catalytic activities of heme enzymes including NOS.[30] Third, the ability that CO binds to ferrous heme of NOS raises a possibility that the gas directly inhibits the enzyme. Although this mechanism is supported by the previous study using purified NOS,[9] it remains unknown whether CO can suppress the NOS activity directly in the endothelial cells. Our current results indicating the acute photo-reversible action of CO on the endothelial NO generation in culture (Figure 6A and 6B) make this possibility

likely. It remains still unknown, through the same mechanism, whether CO generated in the cerebrovascular endothelium could inhibit NO generation in vivo. However, our observation showing an acute action of the endogenous CO suppression on the NO-mediated arteriolar dilatation (Figure 3B) supports the concept that the gas could target the prosthetic heme of NOS3 to inhibit the catalytic activity.

Our immunohistochemical analyses clearly indicate that HO-2 colocalizes with NOS isozymes (Figures 1 and 2). It is this colocalization that enables one gas, CO, to interfere with the formation of another gas, NO, and consequently to antagonize its vasodilatory response. Without such an anatomical arrangement, CO may not be able to change cellular responses mediated by NO. An inhibitory effect of CO on local NO production should be compared with our previous study using transgenic mice that exhibit systemic hypertension through cell-specific HO-1 overexpression in VSMCs.[17] In this case, it is sGC, but not NOS, that colocalizes with the CO-producing enzyme. With this, CO can suppress the activity of sGC in the same VSMC, and by so doing, antagonize NO-mediated vasodilatation. To note is the failure of CO to inhibit NO formation occurring in the neighboring endothelia, minimizing a possibility for CO to exhibit its paracrine effect. This reinforces further the significance of anatomical proximity and leads us to reconsider an ordinary concept that gases freely diffuse through plasma membrane. Indeed, it has been proposed that erythrocyte membrane retards transport of gases such as NO[31] and O_2[32] into the cell by forming a significant diffusion barrier. Such a possibility for CO should be examined further.

Collectively with our previous studies,[2,11,15] CO can regulate vascular tone at least by three distinct ways that depend on microanatomical arrangements of generation and reception of the vasoactive gases. First in the liver, CO modestly stimulates sGC in hepatic stellate cells, thereby reducing the tonic contractile tension of sinusoids where local amount of NO is low.[2,11,33] Second, in resistance arterioles, where there are sufficient amounts of NO, CO could target sGC to interfere with NO-mediated vasodilatation. Previous observation that transgenic mice exhibit systemic hypertension through cell-specific HO-1 overexpression in VSMCs[17] falls into this category. Third, in the cerebral microcirculation, CO interferes with NOS activities as a first step and subsequently reduces NO generation, thereby limiting vasodilatation. Which route, the second or the third, the gas takes to exert its action depends on which enzyme system, either sGC or NOS, HO colocalizes with. Such a notion could explain the complexity of vasoactive actions of CO, which have been reported in experimental models similar to our study: in newborn pigs, either CO or heme-L-lysinate, an exogenous HO substrate, dilates cerebral arterioles,[19] whereas inhibition of HO by chromium mesoporphyrin caused vasodilatation in the same system.[19] Further evaluation of anatomical proximity among the gas-producing enzymes and their reception systems should clarify mechanisms behind these observations.

In conclusion, the current study enables us to unravel physiologic roles of CO or constitutive HO on the regulation of neural and vascular functions in the brain. In view of a recent proposal that HO-2 is an oxygen sensor reducing CO generation in response to a decrease in local O_2 tension,[34,35] an implication could be made on a possible role of the HO isozyme on hypoxia-induced and NO-mediated vasodilatation in the brain.[36–38] Because CO in and around pial microcirculation could be overproduced by an increase in heme as a substrate or by an induction of HO-1 under conditions such as subarachnoid hemorrhage[39] and focal ischemia,[40] aberrant actions of this gas under these pathologic circumstances deserve further investigation.

Acknowledgments

This work was supported by Japan Society for the Promotion of Science, Grant-In-Aid for Scientific Research, 15500267 and 17500261 (to M.K.), Health Labor Sciences Research Grant, Research on Advanced Medical Technology from the Ministry of Health Labor and Welfare, and Grant-in-Aid for Creative Scientific Research, Leading Project for Biosimulation, the 21st Century Center-of-Excellence Program from the Ministry of Education, Culture, Sports, Science and Technology in Japan (to M.S.). We thank Ritsuko Hoshino, Rei Hasegawa, and Kyoko Ishiwata for technical assistance.

References

1. Verma A, Hirsch DJ, Glatt CE, Ronnett GV, Snyder SH. Carbon monoxide: a putative neural messenger. *Science.* 1993;259:381–384.
2. Suematsu M, Goda N, Sano T, Kashiwagi S, Egawa T, Shinoda Y, Ishimura Y. Carbon monoxide: an endogenous modulator of sinusoidal tone in the perfused rat liver. *J Clin Invest.* 1995;96:2431–2437.
3. Suematsu M, Kashiwagi S, Sano T, Goda N, Shinoda Y, Ishimura Y. Carbon monoxide as an endogenous modulator of hepatic vascular perfusion. *Biochem Biophys Res Commun.* 1994;205:1333–1337.
4. Moncada S, Palmer RM, Higgs EA. Nitric oxide: physiology, pathophysiology, and pharmacology. *Pharmacol Rev.* 1991;43:109–142.
5. Ryter SW, Morse D, Choi AM Carbon monoxide: to boldly go where NO has gone before. *Sci STKE.* 2004;2004:RE6.
6. Maines MD. Heme oxygenase: function, multiplicity, regulatory mechanisms, and clinical applications. *FASEB J.* 1988;2:2557–2568.
7. Taille C, El-Benna J, Lanone S, Dang MC, Ogier-Denis E, Aubier M, Boczkowski J. Induction of heme oxygenase-1 inhibits NAD(P)H oxidase activity by down-regulating cytochrome b558 expression via the reduction of heme availability. *J Biol Chem.* 2004;279:28681–28688.
8. Wang J, Lu S, Moenne-Loccoz P, Ortiz de Montellano PR. Interaction of nitric oxide with human heme oxygenase-1. *J Biol Chem.* 2003;278:2341–2347.
9. White KA, Marletta MA. Nitric oxide synthase is a cytochrome P-450 type hemoprotein. *Biochemistry.* 1992;31:6627–6631.
10. Scheele JS, Kharitonov VG, Martasek P, Roman LJ, Sharma VS, Masters BS, Magde D. Kinetics of CO ligation with nitric-oxide synthase by flash photolysis and stopped-flow spectrophotometry. *J Biol Chem.* 1997;272:12523–12528.
11. Suematsu M, Ishimura Y. The heme oxygenase-carbon monoxide system: a regulator of hepatobiliary function. *Hepatology.* 2000;31:3–6.
12. Kajimura M, Shimoyama M, Tsuyama S, Suzuki T, Kozaki S, Takenaka S, Tsubota K, Oguchi Y, Suematsu M. Visualization of gaseous monoxide reception by soluble guanylate cyclase in the rat retina. *FASEB J.* 2003;17:506–508.
13. Koesling D, Friebe A. Soluble guanylyl cyclase: structure and regulation. *Rev Physiol Biochem Pharmacol.* 1999;135:41–65.
14. Kajimura M, Goda N, Suematsu M. Organ design for generation and reception of CO: lessons from the liver. *Antioxid Redox Signal.* 2002;4:633–637.
15. Goda N, Suzuki K, Naito M, Takeoka S, Tsuchida E, Ishimura Y, Tamatani T, Suematsu M. Distribution of heme oxygenase isoforms in rat liver. Topographic basis for carbon monoxide-mediated microvascular relaxation. *J Clin Invest.* 1998;101:604–612.
16. Kyokane T, Norimizu S, Taniai H, Yamaguchi T, Takeoka S, Tsuchida E, Naito M, Nimura Y, Ishimura Y, Suematsu M. Carbon monoxide from heme catabolism protects against hepatobiliary dysfunction in endotoxin-treated rat liver. *Gastroenterology.* 2001;120:1227–1240.

17. Imai T, Morita T, Shindo T, Nagai R, Yazaki Y, Kurihara H, Suematsu M, Katayama S. Vascular smooth muscle cell-directed overexpression of heme oxygenase-1 elevates blood pressure through attenuation of nitric oxide-induced vasodilation in mice. *Circ Res.* 2001;89:55–62.
18. Brian JE Jr, Heistad DD, Faraci FM. Effect of carbon monoxide on rabbit cerebral arteries. *Stroke.* 1994;25:639–643.
19. Leffler CW, Nasjletti A, Yu C, Johnson RA, Fedinec AL, Walker N. Carbon monoxide and cerebral microvascular tone in newborn pigs. *Am J Physiol Heart Circ Physiol.* 1999;276:H1641–H1646.
20. Yamaguchi T, Wakabayashi Y, Tanaka M, Sano T, Ishikawa H, Nakajima H, Suematsu M, Ishimura Y. Taurocholate induces directional excretion of bilirubin into bile in perfused rat liver. *Am J Physiol.* 1996;270: G1028–G1032.
21. Ozawa N, Goda N, Makino N, Yamaguchi T, Yoshimura Y, Suematsu M. Leydig cell-derived heme oxygenase-1 regulates apoptosis of premeiotic germ cells in response to stress. *J Clin Invest.* 2002;109:457–467.
22. Makino N, Suematsu M, Sugiura Y, Morikawa H, Shiomi S, Goda N, Sano T, Nimura Y, Sugimachi K, Ishimura Y. Altered expression of heme oxygenase-1 in the livers of patients with portal hypertensive diseases. *Hepatology.* 2001;33:32–42.
23. Izumi Y, Yamazaki M, Shimizu S, Shimizu K, Yamaguchi T, Nakajima H. Anti-bilirubin monoclonal antibody. II. Enzyme-linked immunosorbent assay for bilirubin fractions by combination of two monoclonal antibodies. *Biochim Biophys Acta.* 1988;967:261–266.
24. Kashiwagi S, Kajimura M, Yoshimura Y, Suematsu M. Nonendothelial source of nitric oxide in arterioles but not in venules: alternative source revealed in vivo by diaminofluorescein microfluorography. *Circ Res.* 2002;91:e55–e64.
25. Kojima H, Nakatsubo N, Kikuchi K, Kawahara S, Kirino Y, Nagoshi H, Hirata Y, Nagano T. Detection and imaging of nitric oxide with novel fluorescent indicators: diaminofluoresceins. *Anal Chem.* 1998;70: 2446–2453.
26. Thomas SR, Chen K, Keaney JF, Jr. Hydrogen peroxide activates endothelial nitric-oxide synthase through coordinated phosphorylation and dephosphorylation via a phosphoinositide 3-kinase-dependent signaling pathway. *J Biol Chem.* 2002;277:6017–6024.
27. Wilson DF, Mokashi A, Chugh D, Vinogradov S, Osanai S, Lahiri S. The primary oxygen sensor of the cat carotid body is cytochrome a3 of the mitochondrial respiratory chain. *FEBS Lett.* 1994;351:370–374.
28. Antonini E, Brunori M. North-Holland Reserch Monographs: Frontiers of Biology. In: Neuberger A, Tatum EL, eds. *The Derivatives of Ferrous Hemoglobin and Myoglobin: Hemoglobin and Myoglobin in Their Reactions With Ligands.* Amsterdam, the Netherlands: North-Holland Publishing Company; 1971:13–39.
29. Stamler JS, Jia L, Eu JP, McMahon TJ, Demchenko IT, Bonaventura J, Gernert K, Piantadosi CA. Blood flow regulation by S-nitrosohemoglobin in the physiological oxygen gradient. *Science.* 1997;276:2034–2037.
30. Haider A, Olszanecki R, Gryglewski R, Schwartzman ML, Lianos E, Kappas A, Nasjletti A, Abraham NG. Regulation of cyclooxygenase by the heme-heme oxygenase system in microvessel endothelial cells. *J Pharmacol Exp Ther.* 2002;300:188–194.
31. Huang KT, Han TH, Hyduke DR, Vaughn MW, Van Herle H, Hein TW, Zhang C, Kuo L, Liao JC. Modulation of nitric oxide bioavailability by erythrocytes. *Proc Natl Acad Sci U S A.* 2001;98:11771–11776.
32. Coin JT, Olson JS. The rate of oxygen uptake by human red blood cells. *J Biol Chem.* 1979;254:1178–1190.
33. Bautista AP, Spitzer JJ. Inhibition of nitric oxide formation in vivo enhances superoxide release by the perfused liver. *Am J Physiol.* 1994; 266:G783–G788.
34. Prabhakar NR, Dinerman JL, Agani FH, Snyder SH. Carbon monoxide: a role in carotid body chemoreception. *Proc Natl Acad Sci U S A.* 1995; 92:1994–1997.
35. Williams SE, Wootton P, Mason HS, Bould J, Iles DE, Riccardi D, Peers C, Kemp PJ. Hemoxygenase-2 is an oxygen sensor for a calcium-sensitive potassium channel. *Science.* 2004;306:2093–2097.
36. Faraci FM, Heistad DD. Regulation of the cerebral circulation: role of endothelium and potassium channels. *Physiol Rev.* 1998;78:53–97.
37. Coney AM, Marshall JM. Role of adenosine and its receptors in the vasodilatation induced in the cerebral cortex of the rat by systemic hypoxia. *J Physiol (Lond).* 1998;509:507–518.
38. Pelligrino DA, Wang Q, Koenig HM, Albrecht RF. Role of nitric oxide, adenosine, *N*-methyl-D-aspartate receptors, and neuronal activation in hypoxia-induced pial arteriolar dilation in rats. *Brain Res.* 1995;704: 61–70.
39. Suzuki H, Kanamaru K, Tsunoda H, Inada H, Kuroki M, Sun H, Waga S, Tanaka T. Heme oxygenase-1 gene induction as an intrinsic regulation against delayed cerebral vasospasm in rats. *J Clin Invest.* 1999;104: 59–66.
40. Bergeron M, Ferriero DM, Vreman HJ, Stevenson DK, Sharp FR. Hypoxia-ischemia, but not hypoxia alone, induces the expression of heme oxygenase-1 (HSP32) in newborn rat brain. *J Cereb Blood Flow Metab.* 1997;17:647–658.

ANTIOXIDANTS & REDOX SIGNALING
Volume 7, Numbers 5 & 6, 2005

Forum Original Research Communication

Hydrogen Sulfide as an Endogenous Modulator of Biliary Bicarbonate Excretion in the Rat Liver

KIMIHITO FUJII,[2] TADAYUKI SAKURAGAWA,[2] MISATO KASHIBA,[1] YASOO SUGIURA,[1] MIEKO KONDO,[1] KAYO MARUYAMA,[1] NOBUHITO GODA,[1] YUJI NIMURA,[2] and MAKOTO SUEMATSU[1]

ABSTRACT

Cystathionine γ-lyase (CSE) is an enzyme catalyzing cystathionine and cysteine to yield cysteine and hydrogen sulfide (H_2S), respectively. This study aimed to examine if H_2S generated from the enzyme could serve as an endogenous regulator of hepatobiliary function. Gas chromatographic analyses indicated that, among rat organs herein examined, liver constituted one of the greatest components of H_2S generation in the body, at 100 μmol/g of tissue, comparable to that in kidney and 1.5-fold greater than that in brain, where roles of the gas in the regulation of neurotransmission were reported previously. At least half of the gas amount in the liver appeared to be derived from CSE, because blockade of the enzyme by propargylglycine suppressed it by 50%. Immunohistochemistry revealed that CSE occurs not only in hepatocytes, but also in bile duct. In livers *in vivo*, as well as in those perfused *ex vivo*, treatment with the CSE inhibitor induced choleresis by stimulating the basal excretion of bicarbonate in bile samples. Transportal supplementation of NaHS at 30 μmol/L, but not that of *N*-acetylcysteine as a cysteine donor, abolished these changes elicited by the CSE inhibitor in the perfused liver. The changes elicited by the CSE blockade did not coincide with alterations in hepatic vascular resistance, showing little involvement of vasodilatory effects of the gas in these events, if any. These results first provided evidence that H_2S generated through CSE modulates biliary bicarbonate excretion and is thus a determinant of bile salt-independent bile formation in the rat liver. *Antioxid. Redox Signal.* 7, 788–794.

INTRODUCTION

CYSTEINE METABOLISM in the liver has been shown to contribute greatly to detoxification processes through multiple mechanisms. Following reduction and decarboxylation processes, this amino acid is converted to taurine, the compound used for conjugation of bile acids. Cysteine serves as a substrate for synthesis of glutathione through reactions of glutamate ligase and glutathione synthase, and is also used to generate sulfate through aspartate transferase and sulfite oxidase; these two compounds have well been shown to play an important role in detoxification of xenobiotics such as acetaminophen. Another important substance generated upon cysteine metabolism *in vivo* is hydrogen sulfide (H_2S). This gaseous compound has recently been shown to account for a signaling molecule in neural and vascular systems. It is produced mainly by two types of pyridoxal 5′-phosphate-dependent enzymes responsible for metabolism of L-cysteine: cystathionine γ-lyase (CSE; EC 4.4.1.1) and cystathionine β-synthase (CBS; EC 4.2.1.22). In other words, although the primary role of the two enzymes is to constitute the transsulfuration pathway that provides cysteine through biotransformation of methionine derived from nutrition, both CSE and CBS are able to use cysteine as the substrate to generate H_2S. The gas synthesized by CBS in brain has been reported to execute neural transduction. On the other hand, CSE-derived H_2S was shown to relax vascular smooth muscle cells through its ability to increase the conductance of potassium channels (22); in this study, H_2S released from the enzyme blocked vasoconstriction of rat aortic rings elicited by glibenclamide, a blocker of the ATP-

[1]Department of Biochemistry and Integrative Medical Biology, School of Medicine, Keio University, Tokyo, Japan.
[2]Division of Surgical Oncology, Department of Surgery, Nagoya University Graduate School of Medicine, Nagoya, Japan.

gated K^+ channel. Furthermore, the CSE activities have been reported to be altered under disease conditions; the activity in the liver is reduced in patients with liver cirrhosis and in those exposed to surgical insults or acquired immune deficiency syndrome (8, 10, 20). On the other hand, experimental models of vitamin B_6 deficiency or streptozotocin-induced diabetes revealed alterations in CSE in the liver under these disease conditions (6, 15). Until now, however, effects of such alterations in the activities on organ functions and roles of H_2S under these circumstances have not been fully investigated yet.

This study was designed to focus first on differences in contribution of CSE to tissue H_2S generation; the data indicated that the liver constitutes one of the largest organ components for the gas generation in the body. Based on this result, we further attempted to examine if H_2S derived from the enzyme could play a role in the regulation of hepatobiliary function. The current results first provided evidence that the liver utilizes this gaseous substance as a modulatory determinant of biliary bicarbonate excretion.

MATERIALS AND METHODS

In vivo *and* ex vivo *determination of bile constituents*

The experimental protocols herein described were approved by our institutional guidelines provided by the Animal Care Committee of Keio University School of Medicine. Male Wistar rats weighing 220–260 g (CLEA Japan, Tokyo, Japan) were allowed free access to laboratory chow and tap water, and were fasted for 24 h prior to experiments. As described elsewhere, rats were anesthetized with an intramuscular injection of pentobarbital sodium at 50 mg/kg, and their common bile ducts were cannulated to collect bile samples. Bile output was monitored *in vivo* according to our previous method (7). When necessary, livers of these rats were perfused *ex vivo* with the oxygenated Krebs–Henseleit buffer at a constant flow rate of 4 ml/min/g of liver in a single-pass mode (14). Bile samples collected through a cannulation were used to determine concentrations of total bile salts, phospholipids, pH values, and bicarbonate (HCO_3^-) according to previous methods described elsewhere (7, 14).

Experimental protocols

Propargylglycine (PPG) was used as a potent inhibitor of CSE. PPG was dissolved in physiological saline as a vehicle and administered intraperitoneally at a dose of 1.5 mmol/kg of body weight at 4 h prior to the preparation for bile duct cannulation. Bile was collected every 10 min until the end of experiments according to our previous method (7). In the case of experiments using the *ex vivo* perfused preparation, livers were excised from the PPG-treated rats and perfused with the Krebs–Henseleit buffer containing 300 μmol/L PPG to avoid a possible reduction of the enzyme blockade due to elimination of the reagent from the system. To examine effects of the intraperitoneal injection of the CSE inhibitor on endogenous H_2S generation, we determined tissue contents of the gas *in vivo*. Livers were excised and snap-frozen at 4 h after the treatment with PPG or vehicle, and the samples were minced with 0.1 *N* NaOH to remove proteins. Amounts of H_2S in the liver tissues were determined by gas chromatography according to previous methods described elsewhere (4). In separate sets of experiments, bile output was monitored every 10 min after establishment of the bile duct cannulation, and concentrations and fluxes of bile constituents were compared between the control and PPG-treated groups. To examine if effects of PPG are attributable to a reduction of the reaction product of CSE such as H_2S, we examined effects of supplementation of NaHS, a soluble donor of the gas at desired concentrations, in the buffer for the *ex vivo* perfusion system. As a control set of the experiments, we compared effects of the same concentrations of *N*-acetylcysteine (NAC), a cysteine donor. In experiments using isolated *ex vivo* perfused livers, sodium taurocholate was added to the buffer at desired concentrations in a range between 0 and 30 μmol/L. Using data collected from these experiments, the bile acid-independent fraction of bile output was determined by plotting bile output as a function of biliary output of bile salts in the samples: the value of the output at the *y*-intercept (zero concentration of bile salts) was regarded as the bile acid-independent fraction (2).

Immunohistochemistry

Liver tissues also served as samples for immunohistochemistry. An anti-CSE antibody was prepared by immunization to rabbit of the C-terminal peptide CYGGTNRYFRRVASE, the sequence of which is identical to that of the rat enzyme. The antibody was purified from the antiserum using affinity chromatography as described elsewhere (3). The specificity of the antibody was confirmed by western blot analyses. For immunohistochemistry, rat livers were removed to prepare OCT compound-embedded frozen sections (7 μm). The sections were immunostained with the anti-CSE antibody using the Vectastain ABC kit (Vector Laboratories), as previously described (5). Semiserial sections were stained with the anti-CSE antibody or with the anti-rat keratin 19 monoclonal antibody (MAB1675; Chemicon, Temecula, CA, U.S.A.) to examine colocalization of the enzyme with biliary epithelium and hepatocellular bile canaliculi, when necessary.

Statistical analyses

The statistical significance of data among different experimental groups was determined by one-way ANOVA and Fisher's multiple comparison test. $p < 0.05$ was considered significant.

RESULTS

Liver constitutes the largest organ component for CSE-derived H_2S generation

Figure 1 illustrates tissue contents of H_2S in different organs. The control liver treated with vehicle contained ~80 nmol/g of tissue of the gas (Fig. 1A). Livers from rats pretreated with 1.5 mmol/kg PPG, an inhibitor of CSE, suppressed the constitutive levels of the gas by 50%. The dose of PPG used in this experiment appeared to be sufficient enough to block the enzyme, as indicated by dose responses of the H_2S contents as a function of doses of the inhibitor (Fig. 1B). When the tissue gas

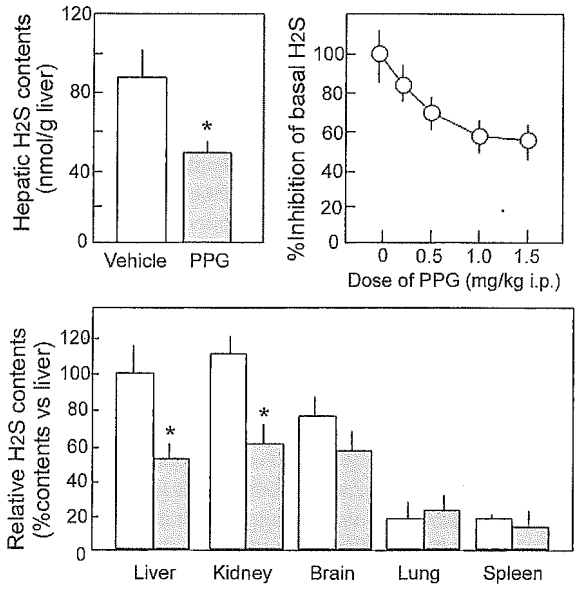

FIG. 1. Effects of administration of PPG, an inhibitor of CSE, on tissue contents of H_2S *in vivo*. (**A**) The effects of the PPG administration on hepatic H_2S contents. PPG was intraperitoneally injected at 1.5 mmol/kg at 4 h prior to the experiments. Data indicate means ± SE of more than eight separate experiments. *$p < 0.05$ as compared with the vehicle-treated control group. (**B**) Dose-dependent effects of PPG on the basal H_2S contents in rat livers. (**C**) Differences in the sensitivity to PPG administration among organs. Open and filled bars represent the tissue H_2S contents in the vehicle- and PPG-treated groups, respectively. Data indicate means ± SE of four separate experiments. *$p < 0.05$ as compared with the vehicle-treated control group.

contents were compared among different organs (Fig. 1C), liver appeared to constitute the largest organ component for endogenous H_2S production; the level was comparable to that measured in the kidney and 1.5-fold greater than that in the brain. So far as judged by sensitivity to PPG, the gas generation in the liver and kidney depended largely on CSE, whereas that in other organs, such as brain, lung, and spleen, seemed CSE-independent; the finding is consistent with previous observations in mouse brain tissues where CBS constitutes a major source for the gas generation (1).

CSE-derived H_2S is a determinant of the basal bile output and biliary HCO_3^- excretion

Figure 2 demonstrates protein expression of CSE in rat liver tissues. Western blot analyses indicated that the purified polyclonal antibody used in this study specifically recognized the enzyme at 40 kDa (Fig. 2A). Immunohistochemistry using the same antibody revealed that the most intense reactivities were seen in periductal regions of portal triads, whereas walls of hepatic arterial walls and terminal portal veins displayed little reactivities, if any. In addition, a modest expression of CSE was notable in hepatocytes, indicating intralobular homogeneity in its expression (Fig. 2B), whereas nonspecific IgG did not stain the slice (Fig. 2C). Figure 2D and E illustrates semiserial sections stained with the anti-CSE and anti-keratin 19 antibodies, respectively. As seen, cytokelatin-positive ductular structures connecting to bile canalicular networks near the portal triad exhibited notable CSE expression, whereas an artery adjacent to the portal vessel did not display evident immunoreactivities. The staining disappeared when the anti-CSE antibody was absorbed by adding the antigen peptide (data not shown).

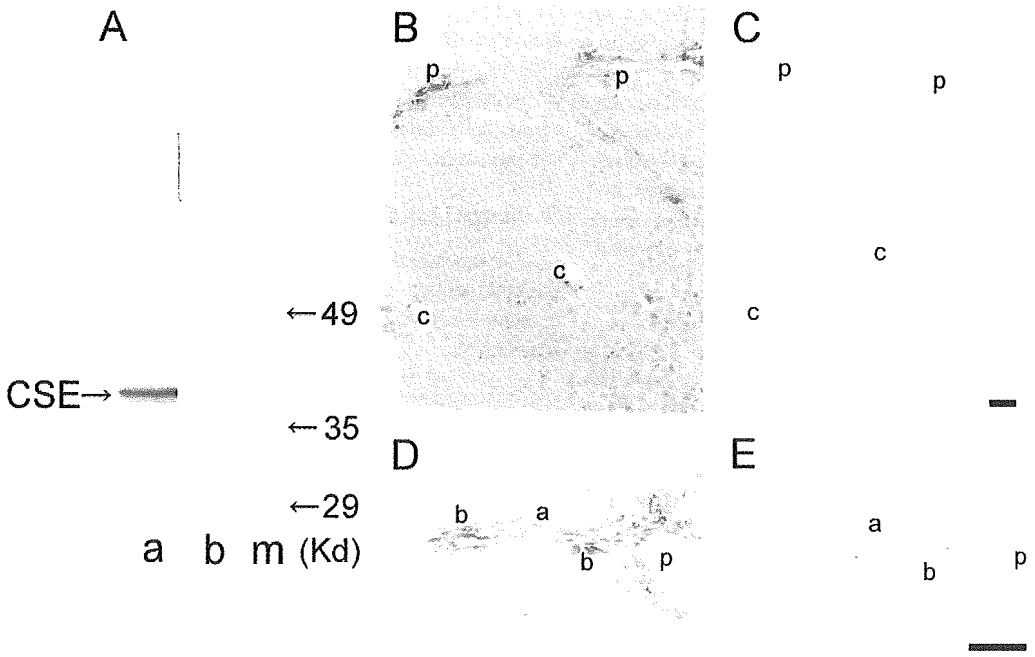

FIG. 2. Expression of CSE in the rat liver. (**A**) western blot analyses using the anti-rat CSE antiserum (lane a) and the affinity column-purified antibody (lane b). m: molecular markers. Note a single band in lane b. (**B** and **C**) Intralobular distribution of CSE in the rat liver stained with the purified anti-CSE antibody and with nonspecific chicken IgG, respectively. p and c: portal and central venules. (**D** and **E**) High magnification of a representative slice stained with the anti-CSE antibody and with the anti-keratin 19 antibody, respectively. a and b: artery and biliary duct. Bars = 50 μm.